Clays and Clay Minerals, Vol. 41, No. 1, 73–86, 1993.

THE INTERCALATION OF KAOLINITE BY ALKALI HALIDES IN THE SOLID STATE: A SYSTEMATIC STUDY OF THE INTERCALATES AND THEIR DERIVATIVES

JOHN G. THOMPSON,[1] NEIL GABBITAS,[1] AND PHILIPPA J. R. UWINS[2]

[1] Research School of Chemistry, Australian National University
Canberra ACT 0200, Australia

[2] Centre for Microscopy and Microanalysis, University of Queensland
QLD 4072, Australia

Abstract—Kaolinite : alkali halide intercalates have been successfully prepared by grinding the salt with kaolinite in the absence of water. Rate of intercalation is shown to correlate negatively with melting point of the salt. The basal dimensions of the intercalates increase with increasing size of the ion. As shown recently for kaolinite : NaCl intercalate, the layered structure survives the dehydroxylation of the kaolinite at 500°–600°C, at which point the excess alkali halide can be removed by rinsing to give an XRD-amorphous material. This amorphous material, of approximate stoichiometry $MAlSiO_4$, reacts at surprisingly low temperatures to give crystalline phases, apparently of the same stoichiometry, with structures closely related to eucryptite (M = Li), carnegieite (M = Na), kalsilite (M = K), and leucite (M = K, Rb, Cs). The relationships between the structures of the reaction products are discussed.

Key Words—Alkali halide, Intercalate, Kaolinite, Structure, Synthesis, XRD.

INTRODUCTION

The ability to intercalate alkali halides with kaolinite has been known since Weiss *et al.* (1966) demonstrated that it was possible using an entraining agent. In another context Miller and Oulton (1972) noted that directly grinding kaolinite with KBr, for the purposes of producing an infrared (IR) disc, caused drastic structural change as observable by IR spectroscopy. Jackson and Abdel-Kader (1978) treated the kaolinite similarly but for a different reason. They observed that dry-grinding of kaolinite with CsCl facilitated the complete intercalation of kaolinite by dimethylsulfoxide (DMSO).

A recent study by the present authors (Thompson *et al.*, 1992) on the kaolinite : NaCl intercalate showed that NaCl could be directly intercalated into kaolinite without the use of an entraining agent. By a combination of dry-grinding of the kaolinite-salt mixture and heating the kaolinite in a saturated aqueous solution prepared from the mixture, it was possible to achieve ≥95% intercalate yield. What was strikingly different between the intercalate generated by this synthetic method and that reported by Weiss *et al.* (1966) was the basal dimension as observed by X-ray powder diffraction (XRD). Thompson *et al.* (1992) observed basal dimensions of 1.25 and 0.95 nm, which we interpreted as a mixture of kaolinite : NaCl intercalates with a double and single layer of NaCl in the interlayer of the kaolinite. In contrast, Weiss *et al.* (1966) reported 1.013 nm for their kaolinite : NaCl intercalate, which was prepared using an entraining agent. It was also notable from their systematic study of all the alkali halides that the basal dimensions of the kaolinite : alkali halide intercalates varied surprisingly little as a function of alkali or halide.

As part of our recent study, we were also able to show that the 1.25 and 0.95 nm layered structure survived by dehydroxylation of the kaolinite at 500°–600°C and that it persists to temperatures above 800°C resulting in a layered tetrahedral framework aluminosilicate. The excess NaCl was removable by rinsing with water, producing an XRD "amorphous" material. When this was heated at 900°C, it recrystallized with a structure very closely related to low-carnegieite, $NaAlSiO_4$ (Klingenberg *et al.*, 1981), some 350°C below its thermodynamic stability field.

The principal motivation for systematically reinvestigating the reaction of kaolinite with other alkali halides was to determine: 1) whether the other alkali halides behaved in the same fashion as NaCl; 2) how the intercalate yield and dimension varied as a function of alkali and halide; and 3) whether they formed derivatives similar to or quite different from those observed for kaolinite : NaCl.

EXPERIMENTAL METHODS

Materials

The kaolinite used in this study was a well-crystallized Georgia kaolinite previously described in Thompson and Cuff (1985) as kaolinite No. 2. The alkali chlorides MCl (M = Li, Na, K, Rb, Cs), other potassium halides KX (X = F, Br, I), and ammonium chloride used in this study were all A.R. grade.

Synthesis

Step 1: *Intercalation.* Initially the kaolinite : alkali halide intercalates (ammonium is considered to be an alkali because of its similar properties) were prepared according to the previous procedure, i.e., by dry-grinding the kaolinite with an excess of salt, dispersing the clay/salt mixture in sufficient distilled water to make a saturated salt solution, then heating to dryness on a hot plate.

In the course of this work, a much simpler and more efficient method of achieving maximum intercalation by the alkali halide was discovered, i.e., that of dry-grinding the kaolinite with an excess of the salt. As a result, we decided to use this dry-grinding method for all specimens in preference to the previously described method. We systematically studied intercalate yield by:

1) varying the grinding time for KCl using two different mills,
2) varying the salt : kaolinite volume ratio for KCl,
3) comparing yield as a function of M in MCl, and
4) comparing yield as a function of X in KX.

For most specimens, we used a bench-top steel ball mill with internal volume of 3 cm^3. For selected specimens, we used a steel geological rock mill with internal volume of ~200 cm^3. The latter mill consisted of a heavy steel cylinder inside a larger radius cylindrical cavity, which resulted in a more severe crushing/grinding action.

Step 2: *Dehydroxylating the intercalate.* The intercalated kaolinite, still in the presence of the excess salt, was heated for 1 hr in a muffle furnace some 20°–30°C below the melting point of the salt or at 700°C, whichever was lower. The LiCl intercalate was only heated to 500°C to prevent the formation of high-eucryptite during this step. In all cases, this was adequate for the dehydroxylation of the kaolinite (~550°C). The ammonium chloride intercalate was not taken beyond Step 1 due to the sublimation temperature of NH_4Cl being 340°C, much less than the dehydroxylation temperature of the kaolinite.

Step 3: *Rinsing to remove excess salt.* The thermally treated specimen was dispersed thoroughly in distilled water then centrifuged to reclaim the reaction product. This step was repeated, typically 5 times, until no further halide ions were detectable in the elute by the addition of silver nitrate solution. Excess water was removed from specimens by heating overnight at 105°C.

Step 4: *Second heating.* The rinsed/dried material was fired overnight at progressively higher temperatures until it was believed that no further structural phase transitions would take place.

Characterization

Intermediate and final reaction products were studied by the following techniques:

1) X-ray powder diffraction (XRD) patterns were collected on a Philips X-ray powder diffractometer using Ni-filtered CuKα(λ = 1.542 Å) with a Sietronics Sie112m automated stepping motor control system.
2) Scanning electron microscopy (SEM) was performed with Jeol 890F and Jeol 6400F scanning electron microscopes, the latter equipped with a Link Si EDS and Moran Scientific Analyser. Samples were analyzed in the SEM without a conductive metal or carbon coating. Scanning electron micrographs shown in Figure 7 were obtained using Pt-coated specimens.
3) Electron microprobe analyses were obtained using a Jeol 8800L electron microprobe operating at 15 kV and 15 mA. Conventional Philibert-Duncumb ZAF corrections were applied to obtain quantitative atomic ratios.

RESULTS

Intercalation

The intercalate yield was most clearly gauged by the reduction in the remnant 7.16 Å kaolinite peak height in the XRD profiles rather than by the increase in intercalate peak heights. Harsh grinding of kaolinite has the effect of reducing preferred orientation due to modification of the platy morphology. This would complicate the measurement of intercalate yield by this method if it were not for the dilution of the kaolinite by the excess alkali halide. The reduction in the 7.16 Å kaolinite peak height was calibrated against a mixture of kaolinite and KCl that had been mixed but not ground.

Varying the grinding time. KCl was selected for this experiment because it gave clearly defined 10.4 and 14.6 Å intercalate peaks in its XRD profile and because both alkali and halide were in the middle of their respective groups in the Periodic Table. Figure 1 shows the XRD profiles (4°–14° 2θ) of the intercalation step for a 1:11 weight ratio (1:14.7 volume ratio) kaolinite : KCl starting mixture for various grinding times using both the bench-top steel ball mill and the geological rock mill. The intercalate yield increased as a function of grinding time. In the ball mill, the intercalate yield varied from 77% after 5 min to 89% after 15 min. In the geological rock mill, which is mechanically more severe, the intercalate yield varied from 90% after 1 min to 95% after 10 min.

Varying the salt : kaolinite volume ratio. Kaolinite : KCl intercalate was chosen for this experiment for the same reasons given above. Figure 2 shows the XRD profiles (4°–14° 2θ) of the intercalation step product for a grind-

https://doi.org/10.1346/CCMN.1993.0410108 Published online by Cambridge University Press

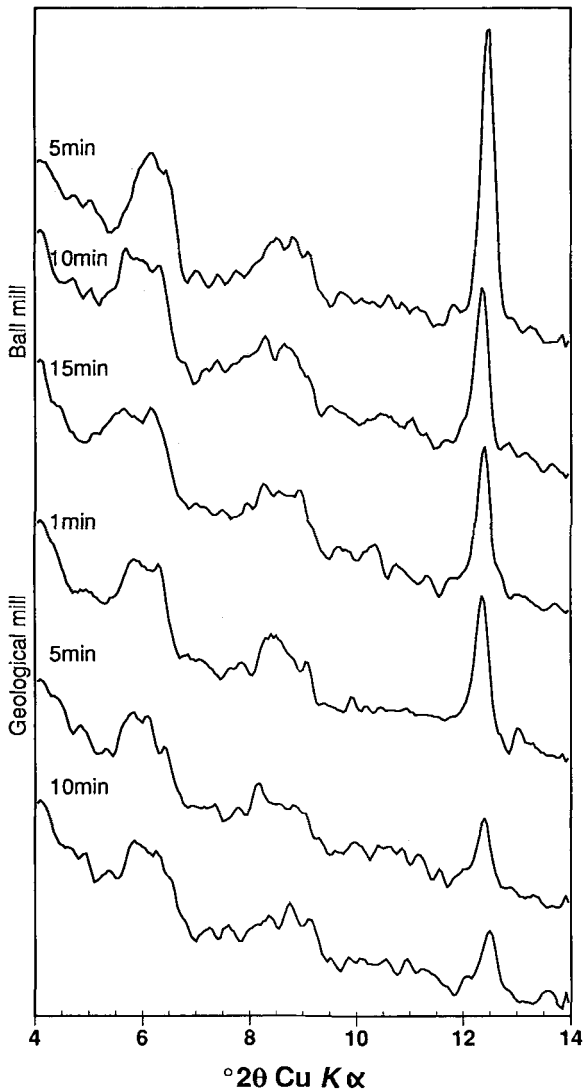

Figure 1. XRD profiles (4°–14° 2θ) of the intercalation step product for a 1:11 weight ratio kaolinite : KCl starting mixture for various grinding times using both the bench-top steel ball mill and the geological rock mill.

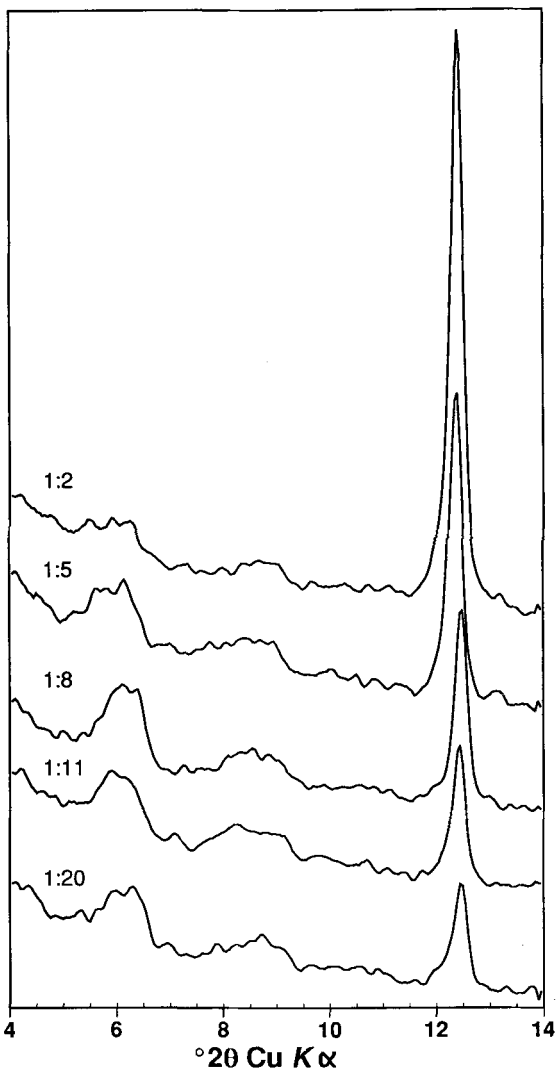

Figure 2. XRD profiles (4°–14° 2θ) of the intercalation step for a grinding time in the bench-top steel ball mill of 5 min for a range of weight ratios of the kaolinite : KCl starting mixture.

ing time in the bench-top steel ball mill of 5 min for a range of weight ratios of the kaolinite : KCl starting mixture. The intercalate yield dramatically increased from ~60% for the 1:2 ratio to ~90% for the 1:20 ratio. Due to the extreme range of dilution of the kaolinite by KCl in these experiments, it was difficult to quantify the yield accurately.

Yield and layer spacing as a function of M in MCl and of X in KX. To study the variation in intercalate yield and layer spacing of the intercalate of the alkali chlorides, we chose a grinding time in the steel ball mill of 5 min with a constant volume ratio of 1:14.7 (corresponding to a 1:11 weight ratio for KCl). Because of the considerable difference in densities of the various alkali halides, it was considered necessary to maintain a constant volume ratio for the results to be meaningful. Figures 3 and 4 show the XRD profiles (4°–14° 2θ) for kaolinite : MCl as a function of M and for kaolinite : KX as a function of X, respectively, all other conditions being the same. For the alkali chloride series, the yield was least for NaCl (75%) and greatest for CsCl (90%); whereas, for the potassium halide series, yield was least for KF (76%) and greatest for KI (93%). Figures 3 and 4 also show the change in layer spacings as a function of M and X. Because some of the intercalate diffraction peaks in these figures were almost unobservable above background, the d-spacings for these peaks were derived from specimens that had been ground for much longer periods than those used in these series. The

https://doi.org/10.1346/CCMN.1993.0410108 Published online by Cambridge University Press

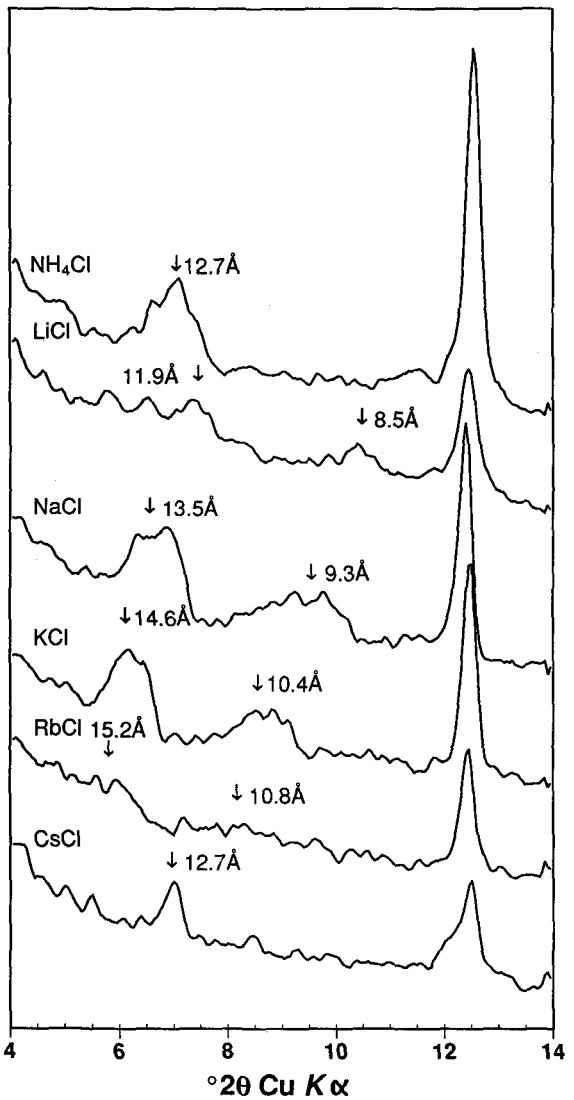

Figure 3. XRD profiles (4°–14° 2θ) for kaolinite : MCl as a function of M, all other conditions being the same. Intercalate d-values have been derived from profiles of specimens ground for much longer periods than those used in this series.

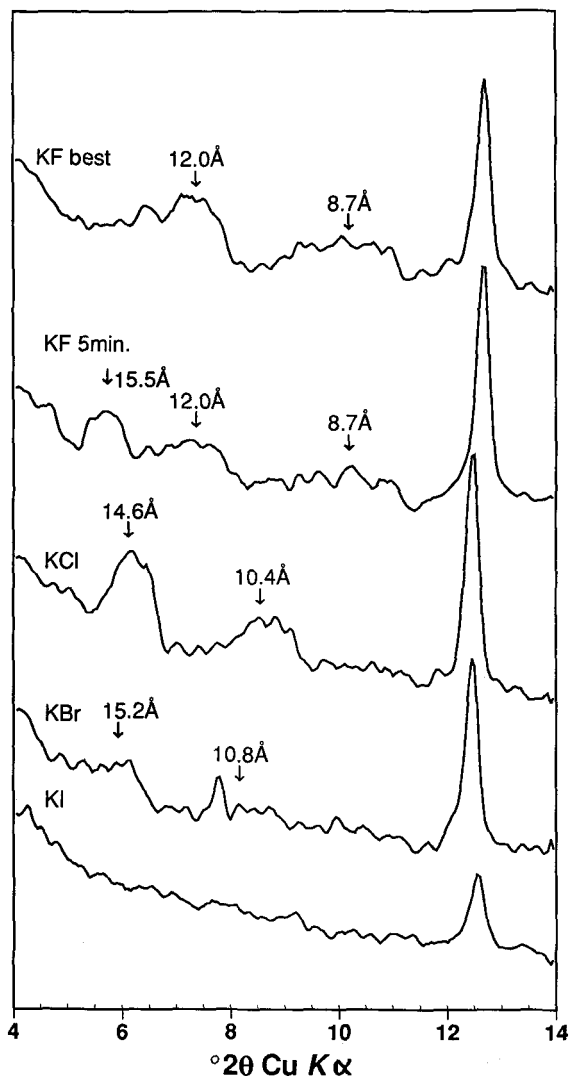

Figure 4. XRD profiles (4°–14° 2θ) for kaolinite : KX as a function of X, all other conditions being the same. Intercalate d-values have been derived from profiles of specimens ground for much longer periods than those used in this series. The profile of an optimized kaolinite : KF intercalate is also shown.

position of peaks was estimated visually from these "best" profiles.

Figure 5 plots the observed intercalate yield against melting point for both MCl, where M = alkali, and KX, where X = F, Cl, Br. In Figure 6, the change in layer spacings as a function of M (top) and X (bottom) can be seen.

Effect of dry-grinding on morphology. In our earlier study of the intercalation of kaolinite by NaCl (Thompson *et al.*, 1992), the kaolinite was preground with the NaCl before heating of the mixture under aqueous conditions to produce the intercalate. The present dry-grinding method of intercalation is mechanically more severe on the kaolinite. Figure 7 presents scanning electron micrographs (secondary electron images) of the starting kaolinite (a) juxtaposed to a kaolinite : NaCl intercalate specimen (~92% yield) that had been thoroughly rinsed to remove all NaCl (b). The dry-grinding modifies the crystal morphology, producing buckled thinner kaolinite sheets. For most crystal aggregates, the original hexagonal crystal form is unrecognisable.

Optimum conditions of synthesis. The conditions used to maximise the formation of intercalate by this dry-grinding method consisted of grinding 10 g of a ~1:15 volume ratio of kaolinite to salt for 15 min in the geological rock mill.

https://doi.org/10.1346/CCMN.1993.0410108 Published online by Cambridge University Press

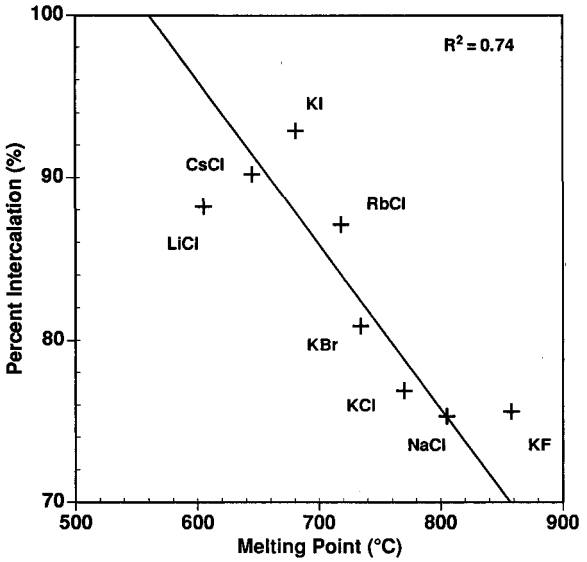

Figure 5. Intercalate yield *vs* melting point of the alkali chlorides and potassium halides with line of best fit.

Dehydroxylating the intercalate

When the intercalated kaolinite was dehydroxylated by heating, the 0.72 nm peak in the XRD profile, corresponding to the ~5% unintercalated material, disappeared. There was no noticeable broad "hump" between 0.45 and 0.30 nm, as observed when kaolinite dehydroxylates to form meta-kaolinite. The intercalate peaks, where observable, persisted through this heating step. As expected from the composition of the mixture, the diffraction peaks due to excess alkali halide dominated the XRD profiles (not shown).

Rinsing to remove excess salt

The XRD profile of the rinsed material was similar for all the alkali halide intercalates. Figures 8–12 show the XRD profiles (14–64° 2θ) of the Step 3 products. The observed intercalate peaks completely disappeared, and a very broad hump between ~0.50 and 0.25 nm (i.e., 18° and 36° 2θ) emerged. With the exception of the KF and LiCl intercalates, the only remaining peak was due to the 3.52 Å peak (25.3° 2θ) of $Al_4Ti_2SiO_{12}$, which is a low-temperature reaction product of anatase-containing kaolinite (Range and Weiss, 1969). Both the KF- and LiCl-derived material showed incipient crystallization of phases to be discussed below.

The absence of any precipitate in the elute upon the addition of silver nitrate solution suggested that all the soluble halide ions had been removed by the rinsing step. EDS analysis of the products usually showed a trace of halide to be present, typically at the level of detection (~1 wt. %). Semiquantitative analysis by EDS indicated that the Step 3 product typically had the stoichiometry $MAlSiO_4$.

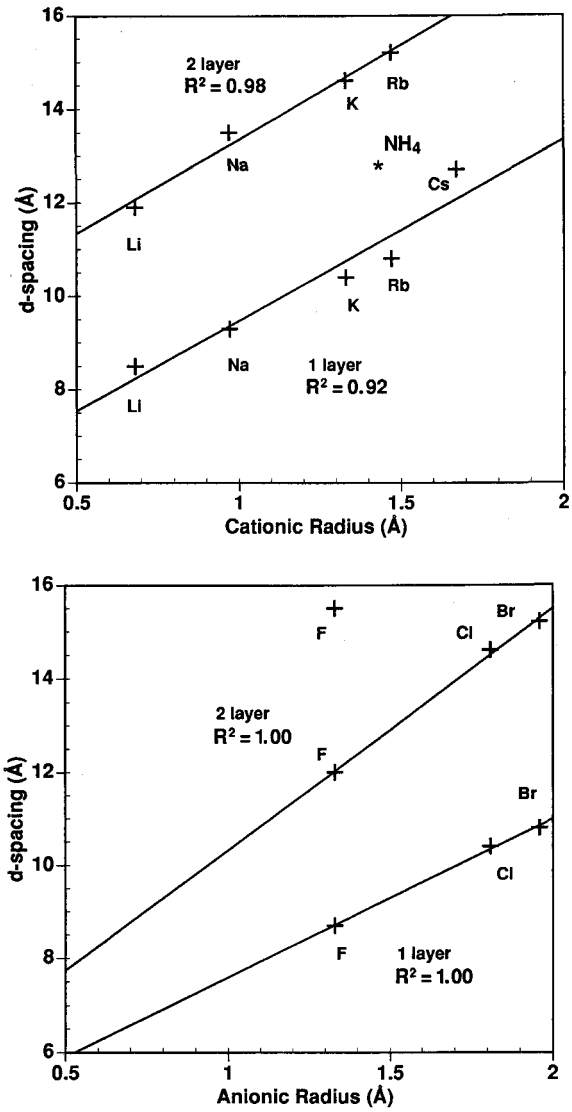

Figure 6. Plots of d-values of intercalates *vs* ionic radius: (top) for MCl, where M = alkali, NH_4 (bottom) for KX, where X = F, Cl, Br with lines of best fit. Intercalate peaks were never observed for KI.

Second heating

The reaction product of Step 3 was heated to progressively higher temperatures. In each case, the XRD-amorphous material reacted to give a well-crystallized material at relatively low temperatures. In some cases, the initial crystal structure gave way to another structure at higher temperatures. The XRD results for each specimen are presented below for each alkali halide. For the quantitative analyses performed using the electron microprobe, the alkali metal compositions are all lower than expected by the formula $MAlSiO_4$; indeed, the lower the melting point the lower the composition. While the alkali metal compositions are given, they are

https://doi.org/10.1346/CCMN.1993.0410108 Published online by Cambridge University Press

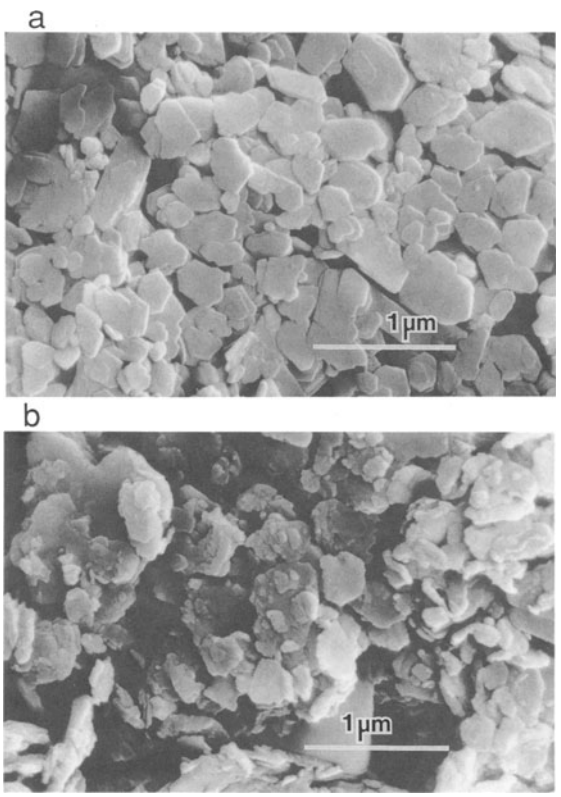

Figure 7. Typical scanning electron micrographs (secondary electron images) of a) the starting kaolinite and b) kaolinite : NaCl intercalate (~92% yield) prepared by dry grinding, which has been subsequently rinsed free of NaCl.

assumed to be underestimated due to volatilization in the electron beam.

LiCl. Figure 8 shows the XRD profile (14°–64° 2θ) of the Step 3 and Step 4 products for LiCl. The set of sharp diffraction lines could be fully indexed to a hexagonal unit cell similar to that for high-eucryptite, $LiAlSiO_4$ (Von Winkler, 1948). The relative intensities were also very similar to those reported. The refined unit cell for the Step 4 product is presented in Table 2. It was first observed at 650°C, though the diffraction lines did not sharpen until 700°C. The temperature at which this phase was formed from the Step 3 product was surprisingly low, given that it is typically prepared either by slowly cooling the melt at ~1500°C (Behruzi and Hahn, 1971) or in the presence of a LiF flux at 920°C (Von Winkler, 1948). As Li has an atomic number of 3, it was not possible to confirm the stoichiometry using EDS in the SEM or electron microprobe.

NaCl. Figure 9 shows the XRD profiles (14°–64° 2θ) of the amorphous Step 3 product and after it was heated at 850°C. The XRD lines could not be indexed to a single unit cell, but the majority of the lines, including all the strong lines, could be indexed to the *F*-centered

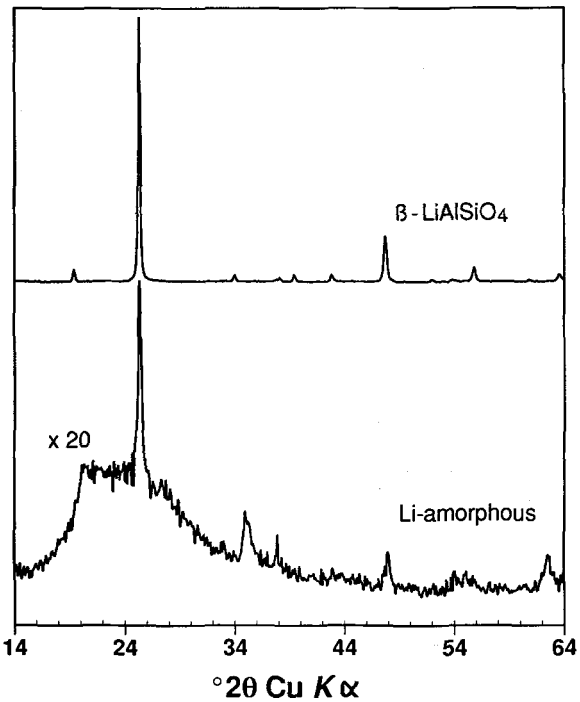

Figure 8. XRD profiles (14°–64° 2θ) of the Step 3 and Step 4 products for LiCl. The amorphous Step 3 product shows incipient formation of high-$LiAlSiO_4$.

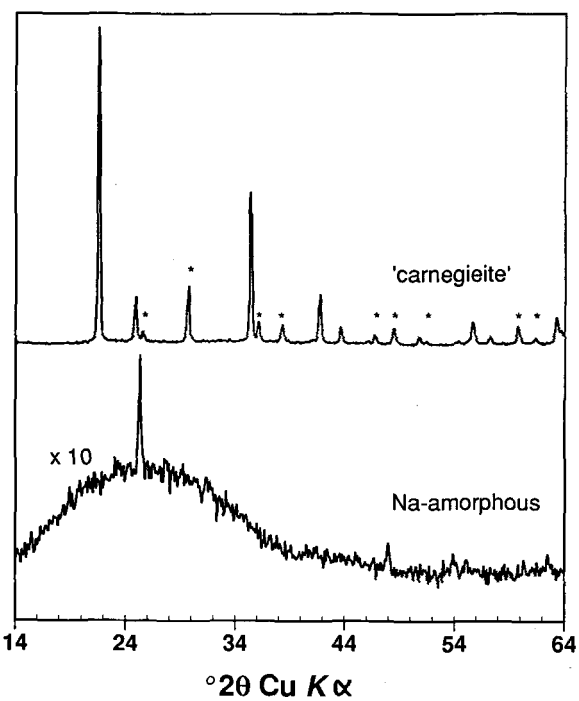

Figure 9. XRD profiles (14°–64° 2θ) of the Step 3 and Step 4 (heated at 850°C) products for NaCl. In the Step 4 product, the asterisks indicate lines that could not be indexed to the cubic "carnegieite" unit cell.

https://doi.org/10.1346/CCMN.1993.0410108 Published online by Cambridge University Press

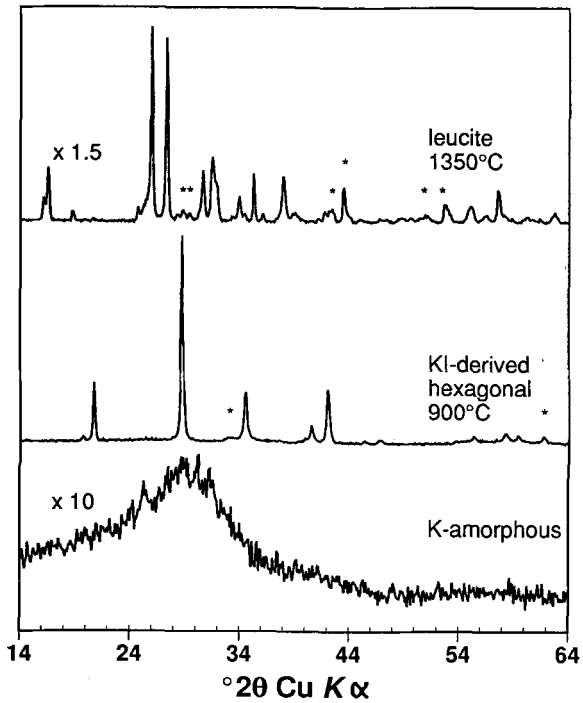

Figure 10. XRD profiles (14°–64° 2θ) of the amorphous Step 3 product for KI, after heating at 900°C, and again after heating at 1350°C. The asterisks indicate lines in the XRD profiles of the KI-derived leucite-like and hexagonal phases that could not be indexed to their respective unit cells.

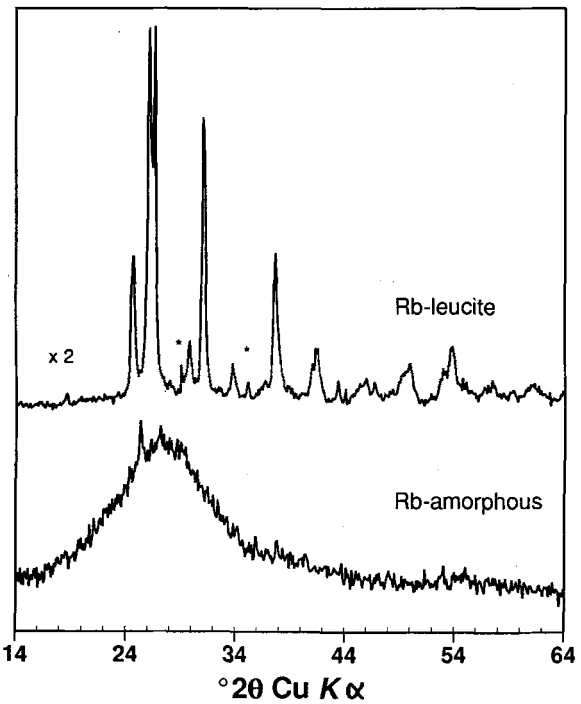

Figure 11. XRD profiles (14°–64° 2θ) of the Step 3 product for RbCl and after heating at 1100°C. The asterisks indicate the two lines in the XRD profile of the RbCl-derived leucite-like phase that could not be indexed to the tetragonal unit cell.

cubic unit cell of high-carnegieite (see Table 2). Quantitative microprobe analysis showed the material to have an average stoichiometry of $Na_{0.82}Al_{0.96}Si_{1.07}$. The low Na content again is attributed to Na loss in the beam. While the Si:Al ratio for this material is reproducibly ~10% high, this is not significantly different from the analysis of the starting kaolinite, which gave a ratio of 1.06 (Table 1). We propose that the XRD lines that could not be indexed to the cubic carnegieite-like unit cell belonged to a second unknown phase with similar stoichiometry.

KF, KCl, KBr, KI. The XRD results for KF, KCl, KBr, and KI were almost identical. Only the profiles for KI are presented. Figure 10 shows the XRD profiles (14°–64° 2θ) of the amorphous Step 3 product for KI and after heating at 900°C and at 1350°C. The 900°C product gave a diffraction pattern that could be indexed to an $a = \sqrt{3}a_{kalsilite}$ hexagonal unit cell with dimensions closely related to those reported for kalsilite, $KAlSiO_4$ (Perrotta and Smith, 1965) (see Table 2). For the KBr- and KI-produced material, the Si:Al ratios were 1.05 and 1.03; whereas, for KF, the ratio was 1.38. This large deviation in Si:Al ratio from the starting material is discussed below.

The 1350°C product gave a quite different diffraction pattern that could be indexed to a tetragonal unit cell similar to that for leucite, $KAlSi_2O_6$ (Faust, 1963). The refined unit cell dimensions of this material and the other KX reaction products are presented for comparison in Table 2. They are not significantly different from that reported for ideal leucite. The main problem with this assignment was the implied stoichiometry. Quantitative microprobe analysis of the leucite-like products for the KCl-, KBr-, and KI-produced material showed that the Si:Al ratio was 1.07–1.13, a figure close to that expected for the formula $KAlSiO_4$ (see Table 1) and much the same as those of starting material and the Step 3 product. While it is possible that the material had unmixed uniformly on a submicron scale, the absence of any compositional inhomogeneity and the lack of XRD evidence for the formation of silica-deficient crystalline phases in the K_2O-SiO_2-Al_2O_3 system suggested that unmixing to give $KAlSi_2O_6$ and $KAlO_2$ had not occurred. For KF the ratio was 1.53, again much higher than expected.

The major difference between KF, KCl, KBr, and KI was the temperature of formation and stability range of both the hexagonal phase, kalsilite, and the tetragonal leucite-like phase. The hexagonal phase was formed at ~800°, 1040°, 985°, and 900°C, respectively. Previously synthetic kalsilite had been prepared hydrothermally at 800°C (Smith and Tuttle, 1957). The kalsilite fully transformed to the leucite-like phase at 1350°,

https://doi.org/10.1346/CCMN.1993.0410108 Published online by Cambridge University Press

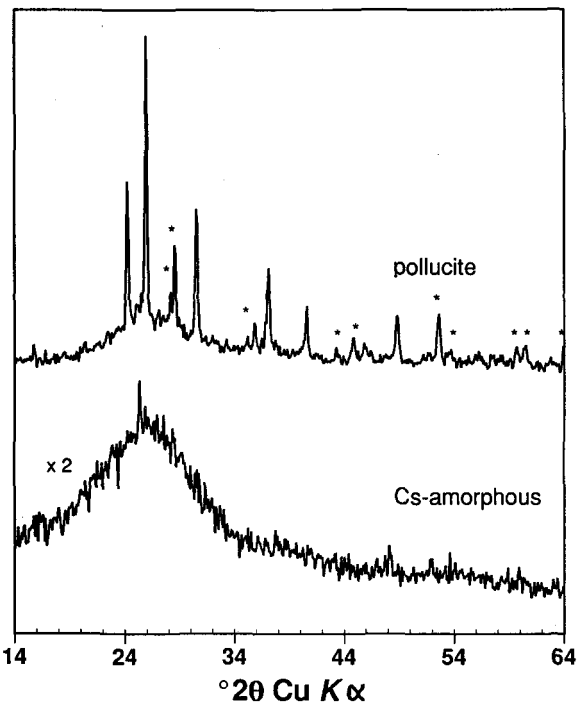

Figure 12. XRD profiles (14°–64° 2θ) of the Step 3 product for CsCl and after heating at 1100°C. The asterisks indicate the lines in the XRD profile of the CsCl-derived leucite-like phase that could not be indexed to the I-centered cubic unit cell.

1060°, 1100°, and 1350°C, respectively. Polymorphism of $KAlSiO_4$ has been investigated previously. Tuttle and Smith (1958) reported that, above ~850°C, kalsilite transformed to an orthorhombic superstructure of kalsilite, which they called O_1. Subsequently, Abbott (1984) proposed that "O_1 is a metastable low-temperature polymorph." Neither study observed a leucite-like phase at this composition.

RbCl. Figure 11 shows the XRD profile (14°–64° 2θ) of the amorphous Step 3 product and after it was heated at 1100°C. This crystalline phase began to appear just below 1100°C. The diffraction peaks could be indexed to a tetragonal unit cell similar to that reported for the Rb analog of leucite, $RbAlSi_2O_6$ (Martin and Lagache, 1975). This material was prepared hydrothermally at 700°C. We note that the strong diffraction peaks at ~28° 2θ coincide with the strongest reflections for a $RbAlSiO_4$ polymorph with a "Immm-type" stuffed tridymite-related structure (Klaska and Jarchow, 1975). The other strong peaks for this phase were absent, suggesting that we did not have this phase. The tetragonal unit cell was subsequently refined and is presented in Table 1. As for KCl above, it is not significantly different from that reported for ideal Rb-leucite. However, quantitative microprobe analysis gave a Si:Al ratio of 1.11, slightly higher than the 1.06 for the starting material but nonetheless close to that expected for the stoichiometry $RbAlSiO_4$.

CsCl. Figure 12 shows the XRD profile (14°–64° 2θ) of the amorphous Step 3 product and after it was heated at 1100°C. This crystalline phase began to appear just below this temperature. The strong diffraction peaks could be indexed to a cubic unit cell similar to that reported for pollucite, $CsAlSi_2O_6$ (Gallagher and McCarthy, 1977), which was prepared by coprecipitation of salts with final firing temperature of 1200°C. Quite a number of XRD lines could not be indexed to the pollucite-like unit cell and were assumed to belong to a second phase. Gallagher *et al.* (1977) had reported a Cs analog to the $RbAlSiO_4$ polymorph with a "Immm-type" structure (Klaska and Jarchow, 1975), though comparison of our data with theirs confirmed that this phase was not present. Microprobe analysis consistently gave a Si:Al ratio of ~1.08. Due to the unreliability of the Cs analysis, it was not possible to resolve the second phase on the basis of composition even though some variation was observed.

DISCUSSION

Structures and reaction mechanisms

While the present study did not exhaustively examine all the alkali halide combinations, it is reasonable to conclude from the results for the alkali chlorides (MCl, where M = alkali, NH_4) and potassium halides (KX, where X = halide) studied that all alkali halides would intercalate to some extent. Even the somewhat hygroscopic salts, KF and LiCl, showed significant intercalation by the dry-grinding method.

In order to propose a mechanism for the room-temperature, mechanically induced intercalation, we should summarize our observations:

1) An excess of alkali halide is necessary to obtain a good yield, and the greater the excess the higher the yield.
2) The lower the melting point of the alkali halide the higher the yield, all other conditions being equivalent.
3) All the alkali halides have a hardness (1.5–3.0 on the Moh scale) comparable to that of kaolinite (2.0–2.5).

SEM images (not presented) showed the kaolinite crystals to be enveloped or coated by the alkali halide. The comparable hardnesses appear to allow the intimate mixing of salt and kaolinite to occur and the large excess of salt appears necessary to completely envelope all the kaolinite crystals. We propose that grinding the kaolinite and salt together causes local "melting" of the alkali halide, generating the very highly polar ion pairs (typically with dipole moment in the gas phase of ~10 Debye), which then proceed to intercalate in a manner similar to small polar molecules, such as DMSO, NMF, and hydrazine. The idea of local 'melting' is supported by the correlation of yield with melting point.

Table 1. Atomic ratios in selected specimens by electron microprobe analysis.

Kaolinite sample "$Al_2Si_2O_7 \cdot 2H_2O$"												
Si	7.0		Al	6.6								
Stoichiometry		$Al_{1.93}$	$Si_{2.04}$									
Hexagonal "$KAlSiO_4$" specimens												
	via KF			via KBr			via KI					
Si	7.0	7.0	6.9	6.4	6.5	6.4	6.1	6.2	6.2			
Al	5.0	5.1	5.1	6.1	6.0	6.2	6.1	5.9	6.0			
K	5.0	4.8	4.9	3.7	3.7	3.5	5.3	5.3	5.4			
Total cation	17.0	16.9	17.0	16.5	16.5	16.4	17.5	17.5	17.6			
Ave. stoichometry	$K_{0.82}$	$Al_{0.84}$	$Si_{1.16}$	$K_{0.61}$	$Al_{1.02}$	$Si_{1.07}$	$K_{0.89}$	$Al_{1.00}$	$Si_{1.03}$			
Carnegieite/leucite-like specimens "$MAlSiO_4$"												
M =	Na			Rb			Cs					
Si	6.5	6.4	6.4		6.7	6.7	6.9	6.7	6.5			
Al	5.7	5.8	5.8	6.8	6.1	6.1	6.2	6.2	6.4			
Na	4.8	5.0	5.0	6.0								
Rb				2.6	2.8	2.6						
Cs							1.9	2.7	2.9			
Total cation	17.0	17.2	17.2	15.6	15.7	15.6	15.0	15.6	15.8			
Ave. stoichometry	$Na_{0.82}$	$Al_{0.96}$	$Si_{1.07}$	$Rb_{0.44}$	$Al_{1.01}$	$Si_{1.12}$	$Cs_{0.42}$	$Al_{1.04}$	$Si_{1.12}$			
M =	K via KF			K via KCl			K via KBr			K via KI		
Si	7.5	7.3	7.6	6.6	6.6	6.6	6.8	6.8	6.8	6.5	6.3	6.1
Al	4.7	5.2	4.6	6.2	6.2	6.2	6.0	6.0	6.0	5.7	5.8	5.9
K	3.7	3.6	3.8	3.2	3.0	3.0	2.5	2.5	2.3	4.8	5.6	5.6
Total cation	16.0	16.0	16.0	16.0	15.8	15.9	15.6	15.5	15.4	17.1	17.7	17.9
Ave. stoichometry	$K_{0.62}$	$Al_{0.81}$	$Si_{1.24}$	$K_{0.51}$	$Al_{1.03}$	$Si_{1.10}$	$K_{0.41}$	$Al_{1.00}$	$Si_{1.13}$	$K_{0.89}$	$Al_{0.97}$	$Si_{1.05}$

Analysis presented on the basis of 24 oxygen atoms. Observed stoichiometries in terms of formula.

Alkali halide intercalate and dehydroxylated intercalate structures and their relationship to kaolinite have been discussed previously (Thompson *et al.*, 1992). Figure 13 shows a schematic polyhedral representation of kaolinite (a), the single layer intercalate (b), and dehydroxylated single layer intercalate (c).

The different intercalate d-spacings observed correspond to single, double, and, for KF, triple layers of

Table 2. Refined and reported unit cell dimensions.

			Refined results		Literature	
			Unit cell dimensions		Unit cell dimensions	
Source	Product	Symmetry	a (Å)	c (Å)	a (Å)	c (Å)
LiCl	high-eucryptite[1]	$P6_1$	5.27(2)	11.06(13)	5.27	11.25
NaCl	high-carnegieite[2]	$F\bar{4}3m$	7.2189(5)		7.325	
RbCl	Rb-leucite-type[3]	$I4_1/a$	13.41(6)	13.64(8)	13.297	13.745
CsCl	pollucite-type[4]	Ia3d	13.73(8)		13.667	
KF	K-leucite-type[5]	$I4_1/a$	13.07(5)	13.78(4)	13.060	13.751
KCl	K-leucite-type[5]	$I4_1/a$	13.09(6)	13.77(9)	13.060	13.751
KBr	K-leucite-type[5]	$I4_1/a$	13.15(5)	13.78(7)	13.060	13.751
KI	K-leucite-type[5]	$I4_1/a$	13.06(5)	13.75(4)	13.060	13.751
KF	kalsilite-type[6]	$P6_3$	9.02(3)	8.58(4)	8.939	8.693
KBr	kalsilite-type[6]	$P6_3$	9.03(3)	8.62(3)	8.939	8.693
KCl	kalsilite-type[6]	$P6_3$	9.06(2)	8.62(3)	8.939	8.693
KI	kalsilite-type[6]	$P6_3$	9.01(2)	8.61(3)	8.939	8.693

[1] Von Winkler (1948).
[2] Smith and Tuttle (1957).
[3] Martin and Lagache (1975).
[4] Gallagher and McCarthy (1977).
[5] Faust (1963).
[6] Perrotta and Smith (1965).

https://doi.org/10.1346/CCMN.1993.0410108 Published online by Cambridge University Press

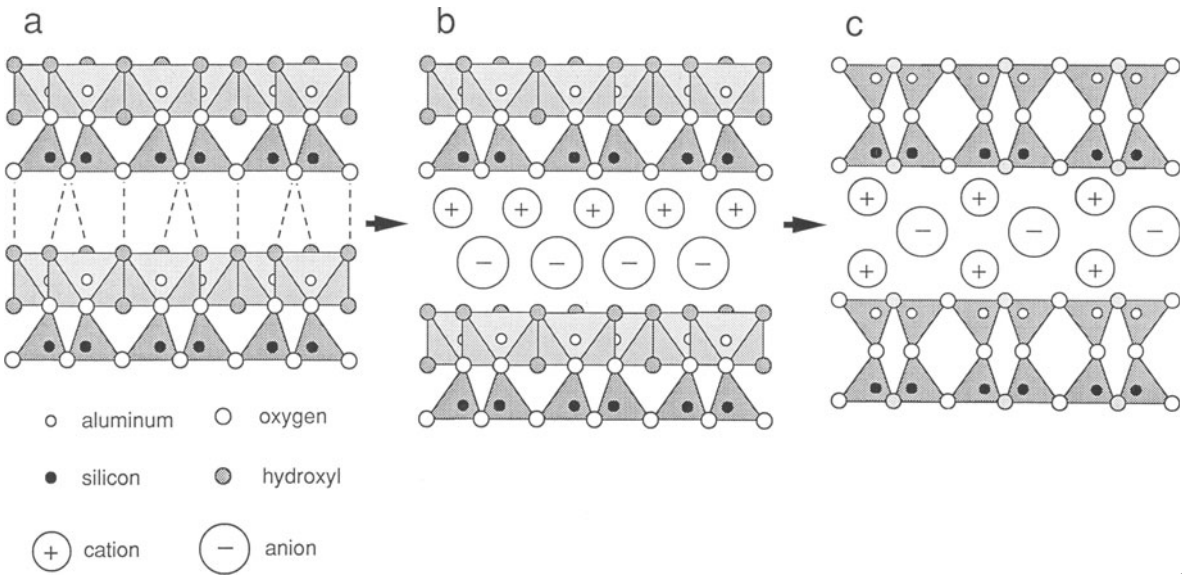

Figure 13. Schematic polyhedral representations of a) kaolinite, b) the single layer intercalate, c) and the dehydroxylated intercalate. The negative charge acquired by the aluminosilicate framework of the dehydroxylated intercalate following dehydroxylation is balanced by excess cations in the interlayer.

alkali halide between the kaolinite sheets. Weiss *et al.* (1966) observed neither multiple intercalate d-spacings nor significant differences between alkali halides. Their results must be attributed to the presence of residual entraining agent between the kaolinite layers.

The observation of anomalously low Si:Al ratios for the material prepared from KF is almost certainly due to reaction of the KF, which is hygroscopic, with the aluminosilicate structure during the dehydroxylation step. The authors have observed that heating kaolinite with KF in aqueous solution results in the ready formation of AlF_3, $KAlF_4$ and K_3AlF_6. Under the experimental conditions described in the present work, we might expect that partial leaching of Al from the kaolinite occurs, resulting in the lower than expected Si:Al ratio.

As the XRD data for all the Step 3 products (Figures 8–12) showed the same broad "amorphous" hump between 18° and 36° 2θ, we conclude that the same destruction of long-range order applies in each case as postulated for kaolinite : NaCl intercalate (Thompson *et al.*, 1992). To explain the observed stoichiometry, we propose the following chemical reaction for the general case of alkali halide during Step 2:

$$Al_2Si_2O_5(OH)_4 \cdot (2 + x)MX \rightarrow 2\,MAlSiO_4 + x\,MX + 2\,HX + H_2O.$$

Due to the presence, after Step 2, of unreacted alkali halide in the interlayer and the excess alkali halide, it is only possible to confirm the stoichiometry of the dehydroxylated kaolinite after all the alkali halide has been rinsed away, i.e., after Step 3. Figure 14a shows a schematic polyhedral representation of the Step 3 product. This model is closely related to the α- or hexacelsian ($BaAl_2Si_2O_8$) structure (Takeuchi, 1958), except that there are twice as many cations between the layers. While α-celsian-type structures give a well-ordered structure with basal spacing of ~7.6 Å, the XRD profile of the rinsed materials showed no evidence of similar long-range order.

The above product can be considered as a reactive form of $MAlSiO_4$, which, when heated to a sufficient temperature, rearranges to produce a framework aluminosilicate structure that can best accommodate the alkali cation, M^+. For the range of alkali metals (M = Li, Na, K, Rb, Cs) we observe the formation of four different structure types. These are summarized below:

M in $MAlSiO_4$	Structure	Structure Type
Li	high-eucryptite	stuffed quartz
Na	high-carnegieite	stuffed cristobalite
K (low-temperature)	kalsilite	stuffed tridymite
K (high-temperature)	leucite	analcime
Rb	Rb-leucite	analcime
Cs	pollucite	analcime

Buerger (1954) was the first to describe the eucryptite, carnegieite, and kalsilite structures as stuffed derivatives of silica polymorphs.

One notable feature of these reaction products is their stoichiometry. Except for the KF-prepared ma-

https://doi.org/10.1346/CCMN.1993.0410108 Published online by Cambridge University Press

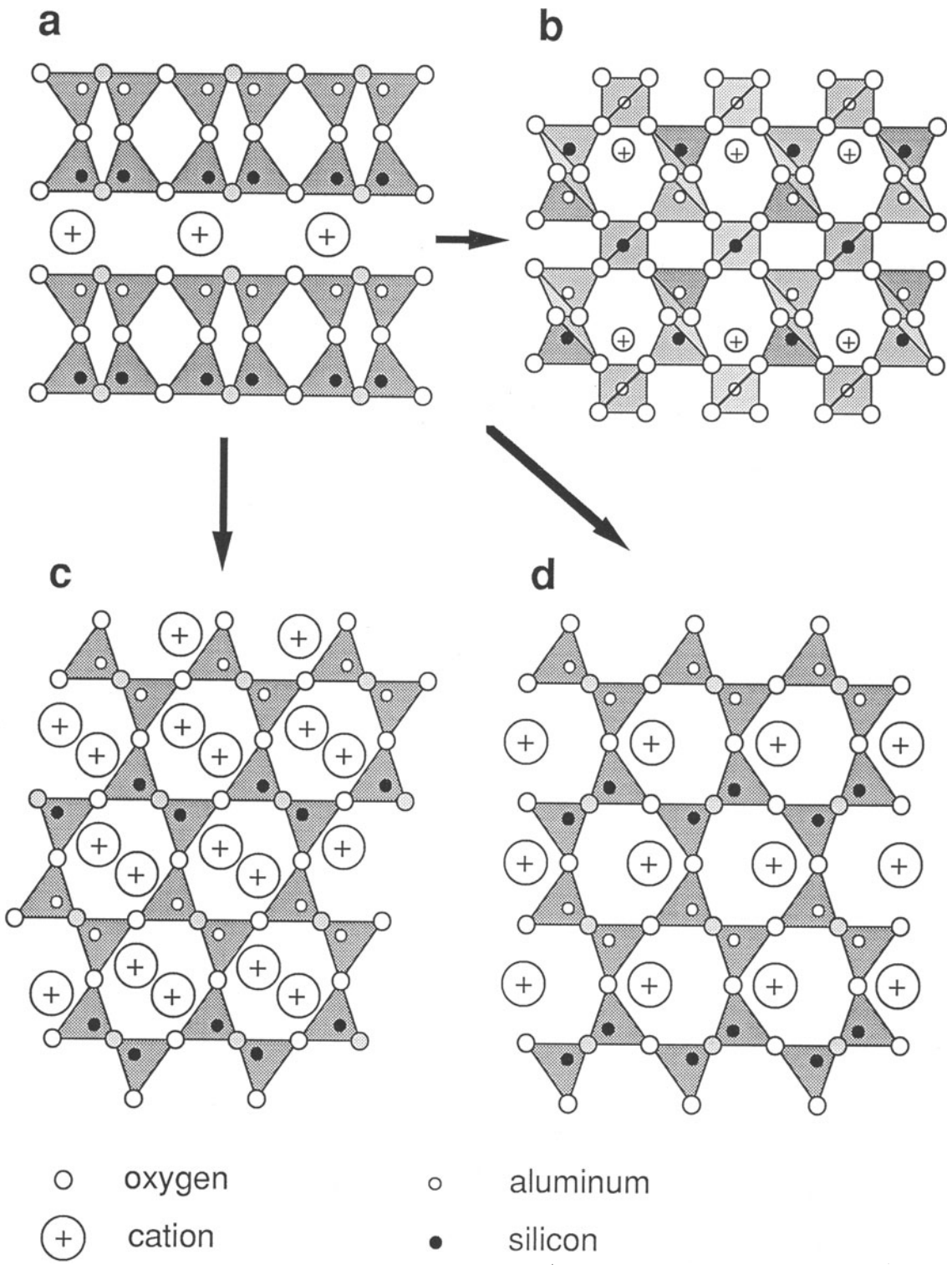

Figure 14. Schematic polyhedral representation of a) the Step 3 (dehydroxylated and rinsed intercalate) reaction product and b) the stuffed quartz, c) cristobalite, and d) tridymite structures. Topotactic transformations from the proposed Step 3 product structure that preserve the Si and Al layering are implied by the arrows.

https://doi.org/10.1346/CCMN.1993.0410108 Published online by Cambridge University Press

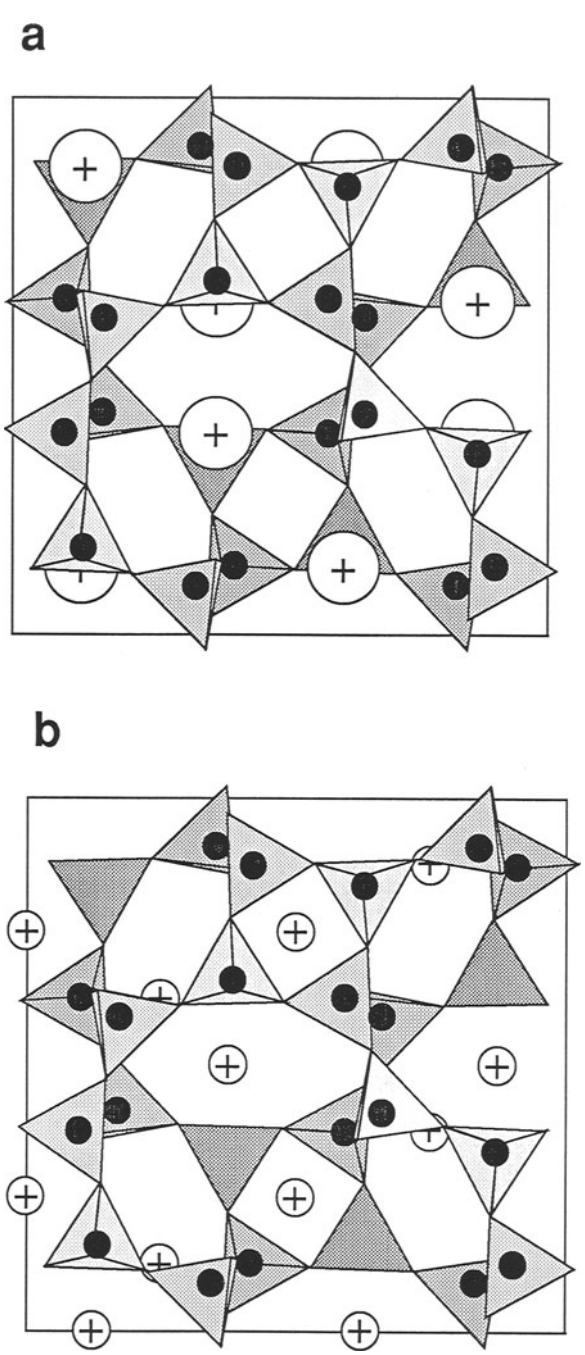

Figure 15. Schematic polyhedral representation of the cubic leucite structure with a) the 16-fold sites occupied and b) the 24-fold sites occupied by monovalent cations.

terial, all the products gave Si:Al ratios consistent with the starting stoichiometry, i.e., the transformation of the XRD-amorphous material to the crystalline phase involved only internal structural rearrangement. This is illustrated in Figure 14 for all but the leucite structure.

Cristobalite and tridymite are both layered structures consisting of hexagonal layers. The layers consist of six-membered rings of corner-sharing SiO_4 tetrahedra, alternately pointing up and down. In Figures 14c and 14d these layers are seen in projection (horizontally) and stacked together (vertically) in two different ways to give either cubic cristobalite-type or hexagonal tridymite-type. Both structures can be simply derived from the proposed Step 3 product structure (Figure 14a) by inversion of alternate tetrahedra within the layers.

In the case of quartz, the transformation from Step 3 product requires significantly more internal rearrangement, as the six-membered rings of tetrahedra are necessarily cleaved to produce the helical arrangement of tetrahedra characteristic of the quartz structure; however, it is clear from Figure 14b that the alternate layers of SiO_4 and AlO_4 tetrahedra proposed for the Step 3 product structure can be preserved in the eucryptite structure.

While quartz is in one sense "layered," the leucite or analcime structure is definitely not. Cubic leucite ($KAlSi_2O_6$) has a typical zeolitic framework of corner-connected $(Si,Al)O_4$ tetrahedra with 4- and 6-membered rings. Its structure is presented schematically in Figure 15a. Only half the unit cell is shown for clarity. As the Step 4 leucite-like products all appeared to have the stoichiometry $MAlSiO_4$, we must consider how the leucite or analcime structure might accommodate the 50% excess alkali cations. In pollucite ($CsAlSi_2O_6$) the space group symmetry is *Ia3d*. The Cs atoms occupy a 16-fold site. There is also a 24-fold site that is either occupied by water or unoccupied. In isostructural analcime ($NaAlSi_2O_6 \cdot H_2O$), the Na atoms occupy two-thirds of the 24-fold site. These alternative cation sites are illustrated in Figure 15b. In the cation-excess leucite-like Step 4 products, if the alkali cations were to occupy these 24-fold sites instead of the 16-fold sites, this would account for the observed stoichiometry. Whether this gives a chemically plausible structure is discussed below in terms of bond-valence sums.

An understanding of the observed structures in terms of Apparent Valences

The relationship between bond length and bond valence in non-molecular solids (Brown and Altermatt, 1985; O'Keeffe, 1989) is now widely accepted. In a given structure, it is possible to calculate the Apparent Valence (AV), i.e., the sum of the bond valences, for an atom using this relationship, namely $s^{ij} = \exp[(r_0{}^{ij} - r^{ij})/B]$, where $r_0{}^{ij}$ and B are empirically determined parameters. These parameters have been tabulated by Brown and Altermatt (1985).

By calculating the AVs for the alkali cations in the cavities of the various structure types, we see that the size of the cavity in the aluminosilicate framework determines which structure type is formed. Table 3

https://doi.org/10.1346/CCMN.1993.0410108 Published online by Cambridge University Press

Table 3. Apparent Valences[1] for various structural models.

	Quartz[2]	Cristobalite[3]	Tridymite[4]	Leucite[5] 16b	Leucite[5] 24c
Li	0.92	0.35	0.16		
Na	2.27	0.93	0.40		0.60
K		2.15	0.97	0.18	1.45
Rb			1.39	0.26	2.08
Cs			2.12	0.40	3.22

[1] Sums of bond valences. R_0 values taken from Brown and Altermatt (1985).

[2] Calculated for eucryptite, $LiAlSiO_4$ (Von Winkler, 1948).

[3] Calculated for low-carnegieite (Withers and Thompson, in press).

[4] Calculated for kalsilite, $KAlSiO_4$ (Perrotta and Smith, 1965).

[5] Calculated for pollucite (Gallagher and McCarthy, 1977).

gives the AVs in the interstitial site(s) in the various structure types for all the alkali cations. In the eucryptite-type structure (stuffed quartz), only Li is small enough to be accommodated by the 4-coordinate site in the helical tunnels. In the carnegieite-type (stuffed cristobalite), the cavity is large enough to fit Na but not K. Kalsilite (stuffed tridymite) has an even larger cavity than carnegieite and comfortably accommodates K but not Rb.

Rb and Cs are too large to fit into the cavities in any of the above structures. A more open zeolite-type structure is necessary. In the cubic leucite structure (space group symmetry *Ia3d*), the two interstitial sites are of very different size. This is illustrated in the AVs listed in Table 3. The pollucite structure, $CsAlSi_2O_6$ structure, has all the 16-fold sites filled (Figure 15a) and, despite the large size of the Cs atom, it is quite underbonded. On the other hand, on the basis of AVs (Table 3), only Na, as observed in analcime, and Li are small enough to fit into the 24-fold sites (Figure 15b). It is evident from these calculations that, for the aluminosilicate leucite framework to accommodate the 50% excess K, Rb, and Cs atoms required by the stoichiometry $MAlSiO_4$, the alkali atoms cannot occupy the 24-fold sites but must partially occupy a general position somewhere between the 16-fold and 24-fold sites. There is no doubt that the large cavity in the leucite framework would be able to accommodate the extra alkali cations.

CONCLUSIONS

The results of this investigation show that all alkali halides can be intercalated into kaolinite directly, i.e., without the need for an entraining agent and in relatively high yield. By not using an entraining agent, it was possible to study systmatically the layer spacing of the intercalates free from complication by the presence of residual entraining agent. The lack of variation in layer spacing reported by Weiss *et al.* (1966) was almost certainly due to this effect.

While the intercalates themselves are unstable in the presence of water they do provide a synthesis route to a range of novel materials. Some of the possibilities have been explored in the present investigation, but the reactivity of the XRD "amorphous" Step 3 product of stoichiometry $MAlSiO_4$ will make it a useful starting material for processes other than simply heating it as we have done.

The crystal structures and crystal chemistry that we have explored provide a useful insight into the way structural features of crystalline materials can be preserved during solid-state chemical reactions. The crystal structures observed for the Step 4 products showed a tendency to preserve both the tetrahedral silicate framework and the alternating layers of Si and Al of kaolinite.

Finally, the synthetic route afforded by the alkali halide intercalate has allowed the formation of two new metastable crystalline phases. Firstly, the stabilization of the high-carnegieite structure with the stoichiometry $NaAlSiO_4$ has not been reported previously, though it is known that an excess of Na_2O does stabilize the cubic structure (Klingenberg and Felsche, 1986). Secondly, the formation of materials with stoichiometry $MAlSiO_4$ with a leucite-like structure has also not been reported previously.

Some preliminary investigations on other metal halide salts suggest that this synthetic route will be more generally applicable than the alkali aluminosilicates studied here.

ACKNOWLEDGMENTS

The authors wish to acknowledge the many helpful discussions with Drs. Ian Mackinnon, Meta Sterns and Ray Withers. We also thank Dr. Christopher Stephens for collecting and processing the electron microprobe data. Support from the Australian Research Council (Grant No. AB9130015 to Drs. I. D. R. Mackinnon and J. G. Thompson) is gratefully acknowledged.

REFERENCES

Abbott, R. N. (1984) $KAlSiO_4$ stuffed derivatives of tridymite: Phase relationships: *Am. Mineral.* **69,** 449–457.

Behruzi, M. and Hahn, T. (1971) High lithium aluminum silicate and related phases in the lithium aluminum silicate, lithium gallium silicate, lithium aluminum germanate, and lithium gallium germanate systems: *Z. Kristallogr.* **133,** 405–421.

Brown, I. D. and Altermatt, D. (1985) Bond-Valence parameters obtained from a systematic analysis of the Inorganic Crystal Structure Database: *Acta Crystallogr., Sect. B* **41,** 244–247.

Buerger, M. J. (1954) The stuffed derivatives of the silica structures: *Amer. Mineral.* **39,** 600–614.

Faust, G. T. (1963) Phase transition in synthetic and natural leucite: *Schweiz. Mineral. Petrog. Mitt.* **43,** 165–195.

Gallagher, S. A. and McCarthy, G. J. (1977) $CsAlSi_2O_6$ *JCPDS data file,* 29-407.

Gallagher, S. A., McCarthy, G. J., and Smith, D. K. (1977)

Preparation and X-ray characterization of cesium aluminosilicate ($CsAlSiO_4$): *Mater. Res. Bull.* **12,** 1183–1190.

Jackson, M. L. and Abdel-Kader, F. H. (1978) Kaolinite intercalation procedure for all sizes and types with X-ray spacing distinctive from other phyllosilicates: *Clays & Clay Minerals* **17,** 157–167.

Klaska, R. Von and Jarchow, O. (1975) Die Kristallstruktur und die Verzwillingung von $RbAlSiO_4$: *Z. Kristallogr.* **142,** 225–238.

Klingenberg, R. and Felsche, J. (1986) Interstitial cristobalite-type compounds $(Na_2O)_{\leq 0.33}$ $Na[AlSiO_4]$: *J. Solid State Chem.* **61,** 40–46.

Klingenberg, R., Felsche, J., and Miehe, G. (1981) Crystal data for the low-temperature form of carnegieite $NaAlSiO_4$: *J. Appl. Crystallogr.* **14,** 66–68.

Martin, R. F. and Lagache, M. (1975) Cell edges and infrared spectra of synthetic leucites and pollucites in the systems potassium aluminum silicate ($KAlSi_2O_6$)–rubidium aluminum silicate ($RbAlSi_2O_6$)–cesium aluminum silicate ($CsAlSi_2O_6$): *Can. Mineral.* **13,** 275–281.

Miller, J. G. and Oulton, T. D. (1972) Prototropy in kaolinite during percussive grinding: *Clays & Clay Minerals* **18,** 313–323.

O'Keeffe, M. (1989) The prediction and interpretation of bond lengths in crystals: *Struct. Bonding* **71,** 161–190.

Perrotta, A. J. and Smith, J. V. (1965) The crystal structure of kalsilite, $KAlSiO_4$: *Min. Mag.* **35,** 588–595.

Range, K. J. and Weiss, A. (1969) Titanium in the kaolinite lattice and formation of pseudoanatase during thermal dissociation of kaolins containing titanium: *Ber. Dtsch. Keram. Ges.* **46,** 629–634.

Smith, J. V. and Tuttle, O. F. (1957) The nepheline-kalsilite system. I. X-ray data for crystalline phases: *Am. J. Sci.* **255,** 282–305.

Takeuchi, Y. (1958) Detailed investigation of the structure of hexagonal $BaAlSi_2O_8$ with reference to its α-β inversion: *Miner. J., Japan* **2,** 311–332.

Thompson, J. G. and Cuff, C. (1985) Crystal structure of kaolinite : dimethylsulfoxide intercalate: *Clays & Clay Minerals* **33,** 490–500.

Thompson, J. G., Uwins, P. J. R., Whittaker, A. K., and Mackinnon, I. D. R. (1992) Structural characterization of kaolinite : NaCl intercalate and its derivatives: *Clays & Clay Minerals* **40,** 369–380.

Tuttle, O. F. and Smith, J. V. (1958) The nepheline-kalsilite system. II. Phase relations: *Am. J. Sci.* **256,** 571–589.

Von Winkler, H. G. F. (1948) Synthesis and crystal structure of eucryptites: *Acta Crystallogr.* **1,** 27–34.

Weiss, A., Thielepape, W., and Orth, H. (1966) Neue Kaolinit-Einlagerungsverbindungen: in *Proc. Int. Clay Conf. Jerusalem, 1966,* **Vol. 1,** L. Heller and A. Weiss, eds., Israel Program for Scientific Translations, Jerusalem, 277–293.

Withers, R. L. and Thompson, J. G. (1993) A modulation wave approach to the structural parameterization and Reitveld refinement of low-carnegieite: *Acta Crystallogr. Sect. B.* (in press).

(Received 17 July 1992; accepted 26 January 1993; Ms. 2242)